Title

Effect of pore penetration on transport through supported membranes studied by electron microscopy and pervaporation

Authors

Shin, Chaeyoung
Jiang, Xi
Ko, Wonjae
et al.

Publication Date

2017-11-01

DOI

10.1016/j.memsci.2017.07.052

Peer reviewed

Journal of Membrane Science 542 (2017) 18–23

Contents lists available at ScienceDirect

Journal of Membrane Science

journal homepage: www.elsevier.com/locate/memsci

Effect of pore penetration on transport through supported membranes studied by electron microscopy and pervaporation

Chaeyoung Shin[a,b], Xi Jiang[c], Wonjae Ko[a], Nitash P. Balsara[a,b,*]

[a] Department of Chemical and Biomolecular Engineering, University of California, Berkeley, CA 94720, USA
[b] Energy Biosciences Institute, University of California, Berkeley, CA 94704, USA
[c] Material Sciences Division, Lawrence Berkeley National Laboratory, Berkeley, CA 94720, USA

ARTICLE INFO

Keywords:
Pore penetration
Supported membrane
Block copolymer
Permeability

ABSTRACT

It has long been recognized that the performance of supported membranes comprising a thin, selective layer and a microporous support layer, is affected by penetration of the selective layer into the porous support. We have attempted to shed light on this phenomenon using a combination of pervaporation experiments and hard angle dark-field scanning transmission electron microscopy (HAADF-STEM). We use a nanophase-separated polystyrene-*b*-polydimethylsiloxane-*b*-polystyrene (SDS) as the selective layer and microporous polytetrafluoroethylene (PTFE) as the support layer. Effective permeabilities of butanol and water were measured as a function of selective layer thickness using a dilute butanol/water mixture as the feed in pervaporation. We were able to estimate the pore penetration layer thickness by comparing experiments with model calculations. We were also able to directly observe the pore penetration by HAADF-STEM. The choice in using a nanophase-separated block copolymer as the selective layer enabled identification of the regions of pore penetration. The pore penetration layer thickness obtained from the HAADF-STEM micrographs corresponded well with estimates based on pervaporation.

1. Introduction

Supported membranes are an increasingly important part of chemical separations [1–4]. They comprise a microporous support underneath a thin, selective, dense membrane. This supported membrane configuration is inevitable in practical applications because flux through the membrane is inversely proportional to thickness; very thin membranes do not have the necessary mechanical properties and thus must be supported. Supported membranes are currently used in numerous applications including gas separation [5,6], water purification [3,7], and pervaporation [8].

A variety of rubbery and glassy homopolymers are used to create the selective thin film depending on the separation process of interest. Examples include polydimethylsiloxane (PDMS), polyimides, and poly (1-trimethylsilyl-1-propyne) (PTMSP) [1,5,9,10]. The microporous support is made out of mechanically rigid and impermeable materials such as polysulfone, polytetrafluoroethylene (PTFE) and ceramic supports [5]. The micron-scale porosity in the support is usually designed so that mass transfer resistance within the support is negligible.

In many cases, the selective membrane material starts penetrating into the pores of the microporous support. This is shown schematically in Fig. 1. While pore penetration improves the adhesion between the selective layer and the support, it also impedes mass transfer. In many practical applications, a third material is added between the selective membrane and the support to control pore penetration. This additional layer is often referred to as the gutter layer. It is widely believed that the patent [11] wherein gutter layers were introduced was crucial for enabling membrane-based separation.

While the importance of pore penetration has long been recognized [12,13], there are relatively few attempts at obtaining direct images of pore penetration. In an important publication, Huang et al. obtained cross-sections of a supported membrane within the pore penetration layer and imaged the resulting surface by SEM [14]. The main purpose of this paper is to report on the morphology of the pore penetration layer in the plane that is perpendicular to the thin film. We accomplish this by using a nanophase-separated block copolymer as the selective layer supported by microporous PTFE. Thin sections of the supported membrane were examined by high angle annular dark-field scanning transmission microscopy (HAADF-STEM). Both nanophase-separation in the selective layer and the imaging modality were essential for obtaining the desired image. We also used the supported membranes to separate butanol from a dilute aqueous solution by pervaporation. We

* Corresponding author at: Department of Chemical and Biomolecular Engineering, University of California, Berkeley, CA 94720, USA.
E-mail address: nbalsara@berkeley.edu (N.P. Balsara).

http://dx.doi.org/10.1016/j.memsci.2017.07.052
Received 30 January 2017; Received in revised form 24 July 2017; Accepted 29 July 2017
Available online 29 July 2017
0376-7388/ Published by Elsevier B.V.

Nomenclature

J_i	flux of i
$P_{i,t}$	permeability of i for the supported membrane
l_t	thickness of the supported membrane
x_i	mole fraction of i in the feed
γ_i	activity coefficient of i in the feed
p_i^{sat}	saturation vapor pressure of i in the feed
y_i	mole fraction of i in the permeate
$p_{permeate}$	pressure in the permeate
α_b	selectivity of butanol
l_s	thickness of the selective layer
l_p	thickness of the pore penetration layer
$P_{i,SDS}$	permeability of i in SDS
A_t	total membrane area
A_p	pore penetration area

measured effective permeability of butanol and water through the supported membrane as a function of membrane thickness. The thickness of the pore penetration layer inferred from transport measurements was consistent with HAADF-STEM results. To our knowledge, this work provides the first direct image of the often assumed supported membrane structure shown in Fig. 1.

2. Methods

2.1. Polymer membrane casting

Polystyrene-*b*-polydimethylsiloxane-*b*-polystyrene (SDS) triblock copolymers of molecular weight 148 kg/mol was purchased from Polymer Source (Dorval, Canada). The molecular weight of the polystyrene (PS) block is each 22 kg/mol, and the molecular weight of the polydimethylsiloxane (PDMS) is 104 kg/mol. The polydispersity index of the polymer is 1.3 and 60 wt% of the polymer is the SDS triblock copolymer, 30 wt% is polystyrene-*b*-polydimethylsiloxane diblock copolymer of molecular weight 22–52 kg/mol, and 9 wt% is homopolymer PS.

Porous polytetrafluoroethylene (PTFE), which was used as the support layer for the supported membrane, was purchased from Sterlitech (Kent, WA). The thickness of the PTFE membrane was 13 μm, and the average pores were 0.2 μm in diameter. By comparing the density of the PTFE membrane to the density of pure PTFE (2.2 g/cm^3 [15]), the volume fraction of the pores in the PTFE was estimated to be 0.20.

Membranes were cast from 2 wt% solutions of SDS and hexane. The SDS/hexane solutions were poured into 100 mL Teflon petri dishes with porous PTFE membranes on the bottom. The Teflon dish was then lightly covered with aluminum foil and a funnel and left to dry for 4–7 days. The membrane thickness was controlled by changing the total amount of solution used in the casting process. The nominally dry supported membranes were placed in a vacuum oven at room temperature for 24 h. In previous studies, we showed that the residual solvent in our dried membranes was below the detection limit of nuclear magnetic resonance (NMR) [16]. The dried membranes were then cut into discs of 37 cm^2 in area and used in pervaporation experiments.

The selective layer thicknesses used in this study range from 1.7 to 125 μm. The thickness of the thickest supported membrane was determined by using a micrometer, and selective layer thickness was determined by subtracting thickness of the support. The soft nature of SDS made direct thickness determination difficult, especially for the relatively thin selective layers. We thus estimated the selective layer thicknesses of the other supported membranes by measuring their masses. We initially assumed that all the mass was contained in the selective layer, and determined the thickness of the pore penetration layer from transport measurements, using the measured mass and thickness of the thickest membrane for calibration. We then corrected the selective layer thickness for the presence of pore penetration and repeated our analysis of the transport data. This iteration was repeated to convergence.

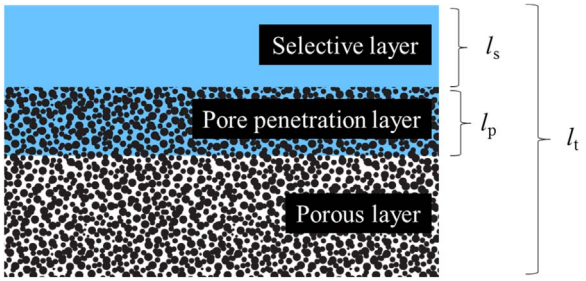

Fig. 1. Schematic of the SDS-PTFE supported membrane cross-section. The selective layer is consisted of SDS, and the pore penetration is consisted of SDS and PTFE. The thicknesses of the selective layer, the pore penetration layer, and the supported membrane are denoted as l_s, l_p, and l_t, respectively.

Table 1
(a) Antoine equation parameters for butanol and water [18], and (b) NRTL equation parameters for butanol and water, denoted as 1 and 2, respectively [19].

(a)		
	Butanol	Water
A	7.838	8.07131
B	1558.19	1730.63
C	196.881	233.426
(b)		
$\Delta g_{12}/R$	$\Delta g_{21}/R$	α
−366.8	1666.4	0.2

2.2. Transmission electron microscopy (TEM)

The 125 μm-thick the SDS-PTFE supported membrane was cryo-microtomed at −160 °C by using Diatome cryo diamond knife and Leica UC6. Sectioned thin films were obtained normal to the plane of the film and imaged by using FEI Tecnai F20 at 200 kV in HAADF-STEM mode at room temperature. We tried a variety of sectioning modes and found that pore collapse within the PTFE support was inevitable. The bright phase in the HAADF-STEM images reflects the presence of PTFE. In addition, images of thin sections of the SDS selective layer were obtained by HAADF-STEM.

2.3. Pervaporation and permeability measurements

A benchtop pervaporation setup (Sulzer) was used to measure permeabilities of the membranes. 2 L feed of butanol-water solutions were used in the experiments. Butanol was purchased from Sigma Aldrich (used as received). The feed solution was circulated at the rate of 6.2 L/min, which corresponds to 1.3 m/s at the membrane surface. Each membrane was left for at least 30 min at the beginning of an experiment to ensure that temperature equilibrium has been reached in the membrane. Vacuum of 2–3 mbar was applied on the other side of the membrane, and the permeate was collected in cold trap with isopropanol and dry ice solution, and the collection time was adjusted so that ~ 0.5 g of permeate would be collected for each time-point. The collected permeate were then thawed, and the mass was measured. The butanol concentration of the permeate was measured by high-performance liquid chromatography (Prominence UFLC instrument, Shimadzu). Four permeate collections was performed for each experiment, and the resulting permeability data from the four collections were averaged.

Effective permeabilities of the SDS-PTFE supported membranes were calculated using solution-diffusion theory [17]:

$$J_i = \frac{P_{i,t}}{l_t}(x_i \gamma_i p_i^{sat} - y_i P_{permeate})$$

where J_i is the flux of species i through the membrane, $P_{i,t}$ is the effective permeability of i for the supported membrane, l_t is the total thickness of the supported membrane, x_i is the mole fraction of i in the feed, γ_i is the activity coefficient of i in the feed, p_i^{sat} is the saturation vapor pressure of i in the feed, y_i is the mole fraction of i in the permeate, and $p_{permeate}$ is the pressure in the permeate. The Antoine equation was used to calculate the activity coefficients (Table 1a) [18], and the non-random two-liquid (NRTL) equation was used to calculate saturation vapor pressures of butanol-water mixtures (Table 1b) [19].

Selectivity of butanol (α_b) is defined as:

$$\alpha_b = \frac{P_{b,t}}{P_{w,t}}$$

where $P_{b,t}$ is the effective butanol permeability and $P_{w,t}$ is the effective water permeability of the SDS-PTFE supported membrane.

Assuming that the selective layer and the pore penetration layer act as mass transfer resistances in series, we arrive at the following relationship:

$$\frac{l_t}{P_{i,t}} = \frac{l_s}{P_{i,SDS}} + \frac{l_p}{P_{i,SDS} A_p / A_t} \quad (3)$$

where l_s and l_p are the thicknesses for the selective layer and the pore penetration layer, respectively, $P_{i,t}$ is the effective permeability of i in the supported membrane, or the permeability that we measure, $P_{i,SDS}$ is the permeability of the SDS, A_t is the total membrane area, A_p is the area that is occupied by the SDS in the pore penetration layer (A_p/A_t = 0.2).

In our initial analysis, we use ls based on the mass of the SDS selective layer as described above. We refer to this as $l_{s,i}$. This enables determination of $l_{p,i}$ from the pervaporation equations. A refined value of the selective layer thickness, $l_{s,r}$, is given by $l_{s,r} = l_{s,i} - 0.2 l_{p,i}$, and the transport data were reanalyzed. This analysis was repeated 4 times until convergence.

3. Results and discussion

The morphology of the SDS selective layer was studied by TEM, and the results are shown in Fig. 2. A disordered bicontinuous morphology comprising dark PS-rich regions and bright PDMS-rich regions is evident. The Fourier transform of the micrograph exhibits a peak at wave vector $Q = Q^* = 0.24\ nm^{-1}$ (Fig. 2b and c), indicating the presence of periodic structure with the characteristic domain spacing, d ($d = 2\pi/Q^*$) of 26 nm. The small angle X-ray scattering (SAXS) profile of a freestanding version of the SDS copolymer was reported in reference [16] and the SAXS profile, shown in Fig. 2c, is qualitatively similar with a Fourier transform of the electron micrograph. Differences in domain spacings between the two techniques (26 versus 35 nm) is attributed to unavoidable distortions during sample preparation for microscopy.

The effective butanol and water permeabilities of SDS-PTFE supported membranes ($P_{b,t}$ and $P_{w,t}$) were measured using a 1 wt% aqueous butanol solution as the feed at four different temperatures: 40, 50, 60, and 70 °C (Fig. 3). The dependence of $P_{b,t}$ and $P_{w,t}$ on selective layer thickness (l_s) is shown in Fig. 3. Both $P_{b,t}$ and $P_{w,t}$ increase with increasing membrane thickness, and start plateauing at around l_s = 40 μm. $P_{b,t}$ of the thickest membrane at 40 °C is eight times of that of the thinnest membrane at 40 °C (Fig. 3a). The permeability difference between the thickest and the thinnest membranes is smaller for $P_{w,t}$; the $P_{w,t}$ of the thickest membrane is four times of that of the thinnest membrane at 40 °C (Fig. 3b). Similar trends are observed at all temperatures, although increase in temperature results in the decrease of permeabilities for all membranes. The increase in temperature also decreases the permeability difference gap between the thickest membrane and the thinnest membrane. At 70 °C, $P_{b,t}$ of the thickest membrane is four times higher than that of the thinnest membrane, and $P_{w,t}$ of the thickest membrane is three times higher than that of the thinnest membrane. The dependence of selectivity on membrane thickness is shown in Fig. 3c; α_b increases from about 3–4 over the thickness ranges covered in this work.

The data in Fig. 3a and b were fit using Eq. (3) with pore penetration layer thickness (l_p), and bulk permeabilities ($P_{b,SDS}$ and $P_{w,SDS}$) as fitting variables. All of the data are consistent with l_p = 2.2 μm, and temperature dependence of bulk permeabilities is shown in Fig. 3d.

We also measured $P_{b,t}$ and $P_{w,t}$ using different feed concentrations (1 wt% and 2 wt% butanol) at 40 °C (Fig. 4). The permeability data are

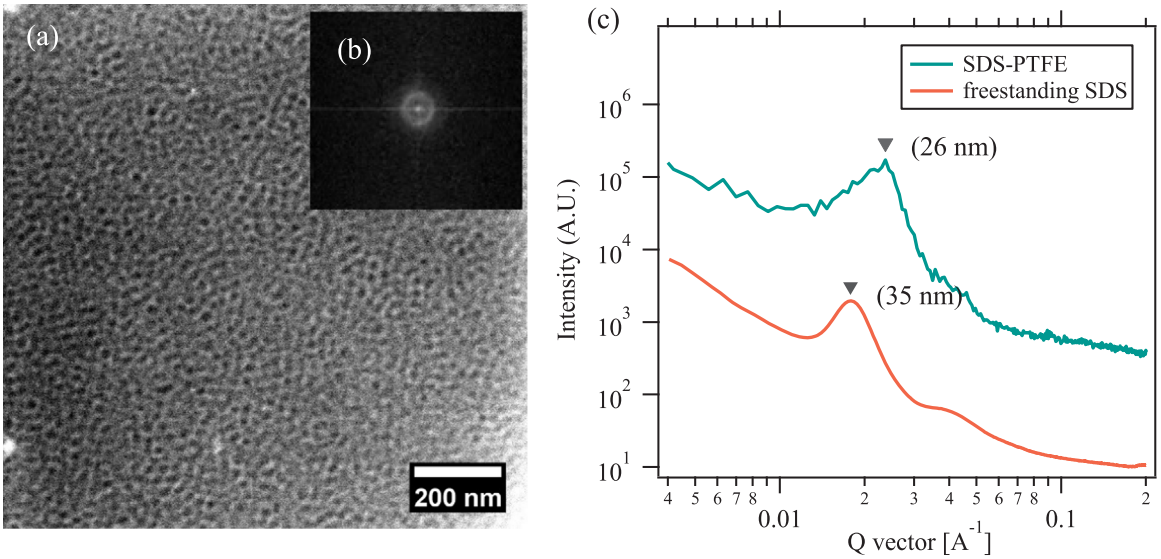

Fig. 2. TEM image of the selective, SDS-only layer of the (a) SDS-PTFE supported membrane. The lighter region is the PDMS phase, and the darker region is the PS phase. (b) The Fourier-transformed image of (a). (c) Azimuthally averaged intensity of (b) plotted as a function of scattering Q vector (green) and small angle X-ray scattering profile of freestanding SDS (red) [14]. Inverted triangles (▼) denote the primary peaks of each curve, from which domain spacings in the parentheses are calculated. (For interpretation of the references to color in this figure legend, the reader is referred to the web version of this article.).

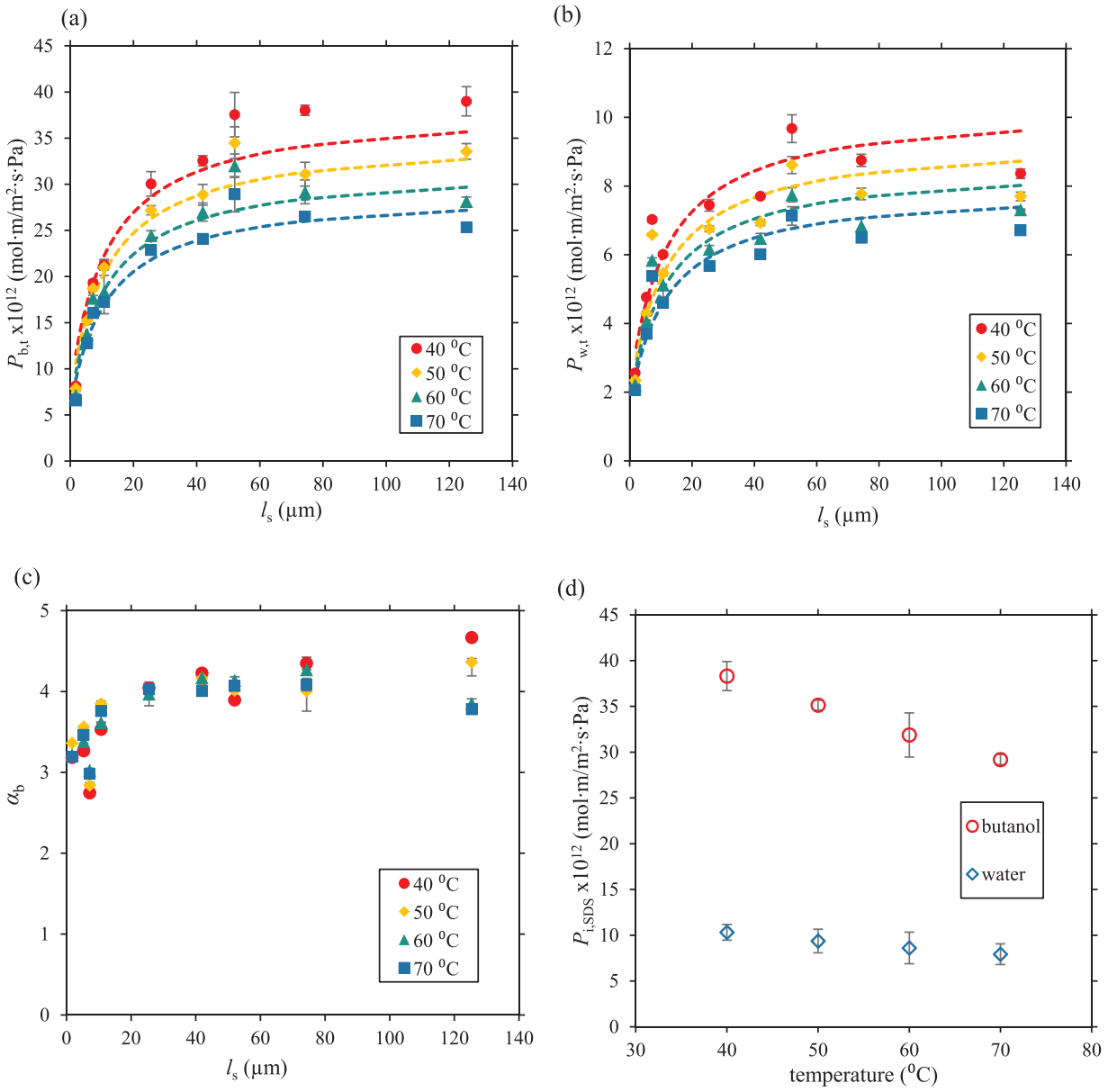

Fig. 3. (a) $P_{b,t}$ (butanol permeability of SDS-PTFE supported membrane), (b) $P_{w,t}$ (water permeability of the SDS-PTFE supported membrane), and (c) α_b (butanol selectivity of the SDS-PTFE supported membrane) plotted as functions of l_s (selective layer thickness). Data obtained at 40 °C ●, 50 °C ◆, 60 °C ▲, and 70 °C ■ are shown with fits using l_p (pore penetration layer thickness) = 2.36 μm in dotted lines. (d) $P_{b,SDS}$ (butanol permeability of SDS, ○) and $P_{w,SDS}$ (water permeability of SDS, ◇) at different temperatures are calculated from l_p = 2.2 μm.

independent of feed concentration, indicating the absence of concentration polarization. This validates the simple model in our data analysis. We note in passing that the slight decrease in α_b with decreasing l_s seen in Fig. 3c is not consistent with our transport model. This inconsistency is observed when the thickness of the supported membrane is comparable to that of the pore penetration layer. While a definitive explanation for this observation is outside the scope of this paper, it is conceivable that the morphology of the block copolymer membrane is affected by film thickness in this regime. Nevertheless, the data in Figs. 3 and 4 indicate the presence of an additional resistance to mass transport in the supported membranes.

Fig. 5 shows cross-sectional TEM images of the unstained SDS-PTFE supported membrane with a 125 μm-thick selective layer. The low magnification micrograph (Fig. 5a) shows the bright support underneath a dark selective layer (the features seen in the active layer are due to the TEM grid). The high magnification micrograph (Fig. 5b) shows the morphology of the active layer (identical to Fig. 5a) and a support layer impregnated with the SDS block copolymer. It is clear that most of the pores in the support layer are filled with the SDS copolymer; one empty pore is evident in the middle of the support layer (Fig. 5b). To our knowledge, Fig. 5b represents the first cross-sectional view of pore penetration in supported membranes. Our use of a nanophase-separated material for selective layer was crucial for distinguishing between the support and material that had penetrated into the pore. The depth of pore penetration observed by TEM (Fig. 5b) was of the order of 1 μm. This is qualitatively consistent with l_p determined from pervaporation (2.2 μm).

4. Conclusion

We have successfully obtained visual evidence of pore penetration in SDS-PTFE supported membranes by HAADF-STEM. The nanophase-separation of SDS block copolymer enabled us to readily identify the regions of pore penetration in the porous PTFE. The pore penetration

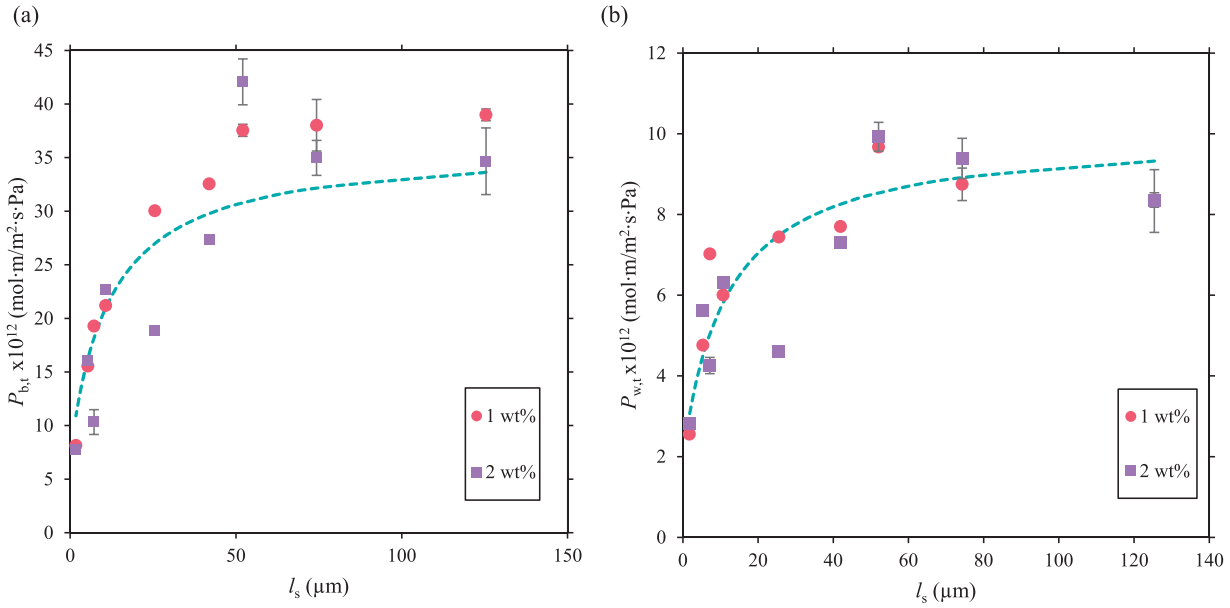

Fig. 4. (a) $P_{b,t}$ and (b) $P_{w,t}$ plotted as functions of l_s at two different butanol feed concentrations: 1 wt% ● and 2 wt% ■. Fits using l_p = 2.36 μm are in dotted lines.

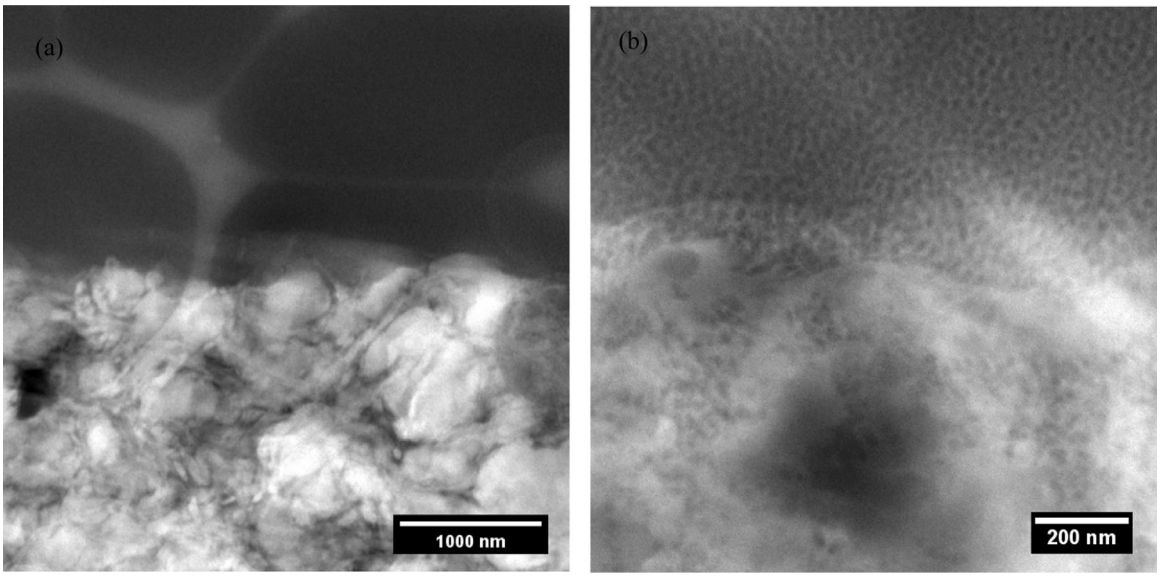

Fig. 5. (a) Cross-sectional TEM image of the SDS-PTFE interface where the bright, bottom region is the porous PTFE and the dark, top region is the SDS. (b) The same membrane cross-section imaged at a higher magnification.

layer thickness (l_p) was also estimated by performing pervaporation experiments using supported membranes with varying selective layer thickness (l_s). l_p estimated from the relationship between permeability and l_s corresponded well with the l_p observed in HAADF-STEM micrographs.

Acknowledgements

The electron microscopy work was supported by the Director, Office of Science, Office of Basic Energy Sciences, Materials Sciences and Engineering Division, of the U.S. Department of Energy under Contract No. DE-AC02-05-CH11231 within the Electron Microscopy of Soft Matter Program (KC11BN). The pervaporation work was supported by the Energy Biosciences Institute, University of California at Berkeley (OO3J04). We thank Professor Benny Freeman for educational discussions.

References

[1] W. Koros, G. Fleming, Membrane-based gas separation, J. Membr. Sci. 83 (1) (1993) 1–80.
[2] D.R. Paul, Y.P. Yampol'skii, Polymeric Gas Separation Membranes, CRC press, 1993.
[3] G.M. Geise, et al., Water purification by membranes: the role of polymer science, J. Polym. Sci. Part B: Polym. Phys. 48 (15) (2010) 1685–1718.
[4] J.T. Arena, et al., Surface modification of thin film composite membrane support layers with polydopamine: enabling use of reverse osmosis membranes in pressure retarded osmosis, J. Membr. Sci. 375 (1) (2011) 55–62.
[5] P. Bernardo, E. Drioli, G. Golemme, Membrane gas separation: a review/state of the art, Ind. Eng. Chem. Res. 48 (10) (2009) 4638–4663.
[6] R.W. Baker, Future directions of membrane gas separation technology, Ind. Eng. Chem. Res. 41 (6) (2002) 1393–1411.
[7] M.A. Shannon, et al., Science and technology for water purification in the coming decades, Nature 452 (7185) (2008) 301–310.
[8] Y. Morigami, et al., The first large-scale pervaporation plant using tubular-type module with zeolite NaA membrane, Sep. Purif. Technol. 25 (1) (2001) 251–260.
[9] L.M. Robeson, Correlation of separation factor versus permeability for polymeric membranes, J. Membr. Sci. 62 (2) (1991) 165–185.
[10] T. Merkel, et al., Gas sorption, diffusion, and permeation in poly

(dimethylsiloxane), J. Polym. Sci. Part B: Polym. Phys. 38 (3) (2000) 415–434.
[11] J.M. Henis, M.K. Tripodi, Multicomponent membranes for gas separations, U.S. Patent No. 4,230,463, 28, 1980.
[12] J.M. Henis, M.K. Tripodi, Composite hollow fiber membranes for gas separation: the resistance model approach, J. Membr. Sci. 8 (3) (1981) 233–246.
[13] F. De Bruijn, et al., Influence of the support layer on the flux limitation in pervaporation, J. Membr. Sci. 223 (1) (2003) 141–156.
[14] R.Y. Huang, X. Feng, Resistance model approach to asymmetric polyetherimide membranes for pervaporation of isopropanol/water mixtures, J. Membr. Sci. 84 (1–2) (1993) 15–27.
[15] C.A. Finch, J. Brandrup, E.H. Immergut (Eds.), Polymer Handbook, third edition, Wiley-Interscience, Chichester, 1989.
[16] C. Shin, et al., Effect of block copolymer morphology controlled by casting-solvent quality on pervaporation of butanol/water mixtures, J. Membr. Sci. 523 (2017) 588–595.
[17] J. Wijmans, R. Baker, The solution-diffusion model: a review, J. Membr. Sci. 107 (1) (1995) 1–21.
[18] J. Gmehling, et al., Vapor-liquid equilibrium data collection, Chemistry data series, vol. I, Flushing, NY, Dechema, 1977.
[19] J.M. Sorensen, W. Arlt, Liquid-liquid equilibrium data collection, Chemical Data series, vol. V, Dechema, 1979.